Available online at www.sciencedirect.com
SCIENCE DIRECT®
Nuclear Instruments and Methods in Physics Research A 544 (2005) 125–133
NUCLEAR INSTRUMENTS & METHODS IN PHYSICS RESEARCH Section A
www.elsevier.com/locate/nima

Three-dimensional numerical studies of the temperature anisotropy instability in intense charged particle beams

Edward A. Startsev*, Ronald C. Davidson, Hong Qin

Plasma Physics Laboratory, Princeton University, Princeton, NJ 08543, USA

Available online 11 March 2005

Abstract

In neutral plasmas with a uniform magnetic field and strongly anisotropic distribution function ($T_{\parallel}/T_{\perp} \ll 1$) an electrostatic Harris-type collective instability may develop if the plasma is sufficiently dense. Such anisotropies develop naturally in accelerators, and a similar instability may lead to a deterioration of the beam quality in a one-component nonneutral charged particle beam. The instability may also lead to an increase in the longitudinal velocity spread, which would make the focusing of the beam difficult and impose a limit on the minimum spot size achievable in heavy ion fusion experiments. This paper reports the results of recent numerical studies of the temperature anisotropy instability using the newly developed Beam Eigenmodes And Spectra (bEASt) code for space-charge-dominated, low-emittance beams with large tune depression ($\nu/\nu_0 \ll 1$). Such high-intensity beams are relevant to next-step experiments such as the Integrated Beam Experiment (IBX), which would serve as proof-of-principal experiment for heavy-ion fusion.

PACS: 29.27.Bd; 52.35.−g; 52.59.Sa

Keywords: Temperature anisotropy instability; Charged-particle beams; Numerical simulation

1. Introduction

It is well known that in electrically neutral plasmas with uniform magnetic field and strongly anisotropic electron distribution ($T_{\parallel e}/T_{\perp e} \ll 1$), where subscript $\parallel$ denotes along the magnetic field, an electrostatic (Harris-like) collective instability may develop if the plasma is sufficiently dense that $\omega_{pe} > \omega_{ce}$, where $\omega_{pe} = (4\pi e^2 n/m)^{1/2}$ is the electron plasma frequency and $\omega_{ce} = eB/mc$ is the electron cyclotron frequency [1]. Such conditions develop naturally in accelerators for heavy-ion beams used for heavy-ion fusion. Indeed, due to conservation of energy for particles with charge e_b and mass m_b accelerated by a voltage V, the energy spread of particles in the beam does not change, and (nonrelativistically) $\Delta E_{bi} = m_b \Delta v_{bi}^2/2 = \Delta E_{bf} = m_b V_b \Delta v_{bf}$, where $V_b = (2e_b V/m_b)^{1/2}$ is the average beam velocity after acceleration.

*Corresponding author.
E-mail address: estarts@pppl.gov (E.A. Startsev).

0168-9002/$ - see front matter © 2005 Elsevier B.V. All rights reserved.
doi:10.1016/j.nima.2005.01.201

Therefore, the velocity spread-squared, or equivalently the temperature, changes according to $T_{\|bf} = T_{\|bi}^2/2e_bV$ (for a nonrelativistic beam). In addition, the transverse temperature may increase due to nonlinearities in the applied focusing field, the self-field forces, nonstationary beam profiles, and beam mismatch. For the case of charged particle beams in accelerators the cyclotron oscillations in the applied magnetic field are replaced by the betatron oscillations of the beam particles in the combined applied and self-generated fields. Heavy-ion fusion experiments require transporting high-current beams when the average depressed betatron frequency of the beam particles is much smaller than the average plasma frequency of the beam particles. The resulting anisotropy-driven instability may lead to a deterioration of the beam quality and an increase in the longitudinal velocity spread, which would make focusing the beam difficult and impose a limit on the minimum spot size achievable in heavy-ion fusion experiments.

Historically, the temperature anisotropy instability in intense charged particle beams was first studied analytically by Wang and Smith [2] for axisymmetric perturbations about the beam with a Kapchinskij–Vladimirskij (KV) distribution assuming infinite anisotropy with $T_{\|b}/T_{\perp b} = 0$. They discovered a large number of unstable modes, some of which are remnants of the unstable transverse spectra of the KV distribution [3]. This work has been recently extended to three-dimensional perturbations by Wang [4]. Since the KV distribution is unstable at sufficiently high beam intensity even for purely transverse perturbations [3], when the temperature anisotropy does not play a role, it was difficult to identify which modes were driven unstable by the temperature anisotropy. The first 3D particle-in-cell simulations of the Harris-type instability in intense beams were carried out by Friedman, et al. [5–7] using the WARP code. They observed a rapid temperature 'equilibration' process of KV beams with large temperature anisotropy. Simulations were carried out for both smooth-focusing and alternating-gradient focusing systems, with qualitatively similar results. Friedman et al., conjectured that the initial rapid heating in the longitudinal direction may be the result of an anisotropy-driven instability reminiscent of the Harris instability in neutral plasmas with the transverse betatron motion replacing the cyclotron motion. Later simulation studies using the WARP code were conducted by Lund, et al. [8,9] using a semi-Gaussian distribution to avoid the numerous unstable modes introduced by the KV distribution, which has a highly inverted distribution in phase space. This paper also reported initial studies of the instability thresholds $(T_{\|b}/T_{\perp b})$ as a function of the depressed tune (v/v_0) for semi-Gaussian and KV distributions. These and other numerical studies [10] of this instability used the electrostatic particle-in-cell (PIC) code WARP, which is sufficiently noisy that resolving the linear stage of instability with sufficient accuracy is very difficult. Also, unlike the KV distribution, the semi-Gaussian distribution is not a rigorous equilibrium solution $(\partial/\partial t = 0)$ of the Vlasov–Maxwell equations about which to perturb. The departure of the initial distribution from a self-consistent equilibrium can inevitably lead to mode excitations which are confused with those due to the anisotropy-driven instability.

In our previous studies of the anisotropy-driven instability in intense beams [11–13], we have addressed the above problems by studying the evolution of perturbations about a bi-Maxwellian distribution, which is a rigorous steady-state equilibrium solution of the Vlasov–Maxwell equations, using the nonlinear perturbative Beam Equilibrium, Stability and Transport (BEST) code [14]. The bi-Maxwellian distribution is known to be a stable equilibrium with respect to transverse perturbations [15], and does not support the spurious modes of the KV distribution. The BEST code implements the nonlinear δf scheme [16] which is fully equivalent to the original nonlinear Vlasov–Maxwell equations. In the δf approach, the simulation particles are used to represent only a small part of the entire distribution $\delta f_b = f_b - f_b^0$, and therefore the noise associated with the representation of the background distribution f_b^0 in conventional particle-in-cell (PIC) simulations is removed. Also, the δf code, operated in the 'linearized' mode, allows the detailed simulation

of the linear stage of the instability. We have also developed a simple analytical theory of the instability for moderately intense beams with bi-Maxwellian distribution [11,12] using the simplified assumption of negligible spread in the depressed betatron frequency, which appears to capture the main features of the instability and is a relatively straightforward generalization of the analysis of the Harris instability to the case of an intense charged particle beam, including the important effects of finite transverse geometry and beam space-charge. The simulation results clearly show that moderately intense beams with normalized depressed tune $0.5<\bar{\nu}/\nu_0\lesssim 0.8$ are linearly unstable to short-wavelength perturbations with $k_z^2 r_b^2 \gtrsim 1$, provided the ratio of longitudinal and transverse temperatures is smaller than some threshold value.

In this paper we extend our previous simulation studies of this instability [11–13] to the case of space-charge-dominated, low-emittance beams with $\bar{\nu}/\nu_0<0.5$. Such high-intensity beams are relevant to next-step experiments such as the Integrated Beam Experiment (IBX) which would serve as a proof-of-principal experiment for heavy-ion fusion. To investigate detailed linear stability properties numerically, we make use of the newly developed Beam Eigenmodes And Spectra (bEASt) code described below.

2. Instability mechanism

In the following analysis, it is convenient to introduce the effective *depressed* betatron frequency $\omega_{\beta\perp}$. For simplicity, the analysis is carried out in the beam frame ($V_b=0$). It can be shown [17] that for the bi-Maxwellian equilibrium distribution assumed in Eq. (17), the mean-square beam radius r_b^2 defined by

$$r_b^2=\langle r^2\rangle=\frac{\int \mathrm{d}r\, r^3 n_b^0(r)}{\int \mathrm{d}r\, r n_b^0(r)} \tag{1}$$

is related exactly to the line density $N_b=2\pi\int \mathrm{d}r\, r n_b^0(r)$, and the transverse beam temperature $T_{\perp b}$ by the equilibrium radial force balance equation [17]

$$\omega_f^2 r_b^2=\frac{N_b e_b^2}{m_b}+\frac{2T_{\perp b}}{m_b} \tag{2}$$

where $r_b^2=\langle r^2\rangle$ is the mean-squre radius, e_b and m_b are the charge and mass, respectively, of a beam particle and $\omega_f=\text{const.}$ is the transverse frequency associated with the applied focusing field in the smooth-focusing approximation. Eq. (2) can be rewritten as

$$\left(\omega_f^2-\frac{1}{2}\bar{\omega}_{pb}^2\right)r_b^2=\frac{2T_{\perp b}}{m_b} \tag{3}$$

where we have introduced the effective *average* beam plasma frequency $\bar{\omega}_{pb}$ defined by

$$r_b^2\bar{\omega}_{pb}^2\equiv\int_0^{r_w}\mathrm{d}r\, r\omega_{pb}^2(r)=\frac{2e_b^2N_b}{m_b}. \tag{4}$$

Then, Eq. (3) can be used to introduce the effective average *depressed* betatron frequency $\omega_{\beta\perp}$ defined by

$$\omega_{\beta\perp}^2\equiv\left(\omega_f^2-\frac{1}{2}\bar{\omega}_{pb}^2\right)=\frac{2T_{\perp b}}{m_b r_b^2}. \tag{5}$$

The normalized tune depression $\bar{\nu}/\nu_0$ is defined by

$$\frac{\bar{\nu}}{\nu_0}\equiv\frac{\omega_{\beta\perp}}{\omega_f}=(1-\bar{s}_b)^{1/2} \tag{6}$$

where $\bar{s}_b\equiv\bar{\omega}_{pb}^2/2\omega_f^2$ is the normalized beam intensity.

We now illustrate the physical mechanism for the electrostatic Harris instability in intense particle beams with a KV distribution. As shown in Section 3, the dipole mode has the highest growth rate. Therefore, to illustrate the instability mechanism, we consider dipole-mode perturbations which in lowest order correspond to a rigid displacement of the beam centroid in the transverse x-direction (for example). Since a KV beam has a uniform density profile, the perturbation of the electrostatic potential inside the beam has the form

$$\delta\phi(\mathbf{x},t)=\hat{\phi}\,\frac{x}{r_b}\exp(\mathrm{i}k_z z-\mathrm{i}\omega t) \tag{7}$$

where $\hat{\phi}$ is the perturbation amplitude, ω and k_z are the perturbation frequency and the longitudinal wavenumber, respectively. We show in Section 3 that the growth rate is an increasing

function of $k_z r_b$ and approaches its limiting value for $k_z^2 r_b^2 \gg 1$. Therefore, in what follows it is assumed that $k_z^2 r_b^2 \gg 1$, and that the perturbation in electric field is given approximately by $\delta \boldsymbol{E} = -\mathrm{i} k_z \delta\phi \boldsymbol{e}_z$.

Next, we consider a beam particle oscillating longitudinally in the perturbed electric field and at the same time performing transverse betatron oscillations. For arbitrary distribution function, the equilibrium self-electric field is nonlinear, and the transverse betatron oscillation of the beam particles will contain many harmonics of the betatron frequency, which generally depends on the particle energy and angular momentum. For purposes of illustrating the physical mechanism, we consider here the simplified model of equivalent KV beam where all of the particles oscillate with the same frequency, equal to the average depressed betatron frequency $\omega_{\beta\perp}$ defined in Eq. (5), i.e.,

$$x(t) = \hat{x}\cos(\omega_{\beta\perp} t + \alpha_0) \tag{8}$$

where α_0 is the oscillation phase at $t = 0$ and $\hat{x} = \sqrt{2H_x/m_b}/\omega_{\beta\perp}$ is the oscillation amplitude.

Making use of Eqs. (7) and (8), the longitudinal equation of motion for a beam particle becomes

$$\ddot{z} = -\mathrm{i} k_z \frac{e_b}{m_b}\,\hat{\phi}\,\frac{\hat{x}}{r_b}\cos(\omega_{\beta\perp} t + \alpha_0)\mathrm{e}^{\mathrm{i}k_z z_0 - \mathrm{i}\omega t} \tag{9}$$

where we have assumed that beam is cold in longitudinal direction. Integrating Eq. (9) with respect to time, we obtain

$$\begin{aligned} z_\alpha &= \mathrm{i} k_z \frac{e_b}{m_b}\,\hat{\phi}\,\frac{\hat{x}}{2r_b} \\ &\quad\times\left[\frac{\mathrm{e}^{\mathrm{i}\alpha}}{(\omega-\omega_{\beta\perp})^2} + \frac{\mathrm{e}^{-\mathrm{i}\alpha}}{(\omega+\omega_{\beta\perp})^2}\right]\mathrm{e}^{\mathrm{i}k_z z_0 - \mathrm{i}\omega t} \end{aligned} \tag{10}$$

where $\alpha = \alpha_0 + \omega_{\beta\perp} t$. To calculate the average displacement $\langle z\rangle(x,z,t)$ in the z direction we average over all particles with the same transverse position x at time t. This gives

$$\begin{aligned} \langle z\rangle(x,z,t) &= \frac{1}{2}(z_\alpha + z_{-\alpha}) \\ &= \mathrm{i} k_z \frac{e_b}{m_b}\,\hat{\phi}\,\frac{x}{2r_b} \\ &\quad\times\left[\frac{1}{(\omega-\omega_{\beta\perp})^2} + \frac{1}{(\omega+\omega_{\beta\perp})^2}\right]\mathrm{e}^{\mathrm{i}k_z z - \mathrm{i}\omega t} \\ &= -\frac{e_b \delta E_z}{2m_b} \\ &\quad\times\left[\frac{1}{(\omega-\omega_{\beta\perp})^2} + \frac{1}{(\omega+\omega_{\beta\perp})^2}\right] \end{aligned} \tag{11}$$

where $\delta E_z = -\mathrm{i} k_z \delta\phi$ [see Eq. (7)]. Note that even though the individual particle motion [Eq. (10)] has two characteristic frequencies, $\omega - \omega_{\beta\perp}$ and $\omega + \omega_{\beta\perp}$, the average quantity $\langle z\rangle$ oscillates at the perturbation frequency ω [Eq. (11)]. From the continuity equation for the density perturbation,

$$\frac{\partial \delta n}{\partial t} + \frac{\partial}{\partial z}\left(n_0 \frac{\partial\langle z\rangle}{\partial t}\right) = 0 \tag{12}$$

we obtain

$$\delta n = -n_0 \frac{\partial\langle z\rangle}{\partial z}. \tag{13}$$

Substituting Eqs. (11) and (13) into Poisson's equation $\boldsymbol{\nabla}\cdot\delta\boldsymbol{E} \simeq \partial\delta E_z/\partial z = 4\pi e_b \delta n$, we obtain the dispersion relation

$$1 = \frac{\bar{\omega}_{pb}^2}{2}\left[\frac{1}{(\omega-\omega_{\beta\perp})^2} + \frac{1}{(\omega+\omega_{\beta\perp})^2}\right] \tag{14}$$

where we have made use of the average value of plasma frequency introduced in Eq. (4) to take into account the beam density profile shape in a lowest-order sense. Using the definition of the depressed tune [Eqs. (5) and (6)], we can rewrite Eq. (14) as

$$\frac{\nu_n^2}{1-\nu_n^2} = \left[\frac{1}{(\omega_n/\nu_n - 1)^2} + \frac{1}{(\omega_n/\nu_n + 1)^2}\right] \tag{15}$$

where $\nu_n = \bar{\nu}/\nu_0$ is the normalized depressed tune, and $\omega_n = \omega/\omega_f$ is the normalized mode frequency. Eq. (15) is easily solved to give

$$\omega_n^2 = 1 \pm \sqrt{(1-\nu_n^2)(1+3\nu_n^2)}. \tag{16}$$

From Eq. (16), we obtain that for $\nu_n < \nu_n^{th} = \sqrt{2/3} \approx 0.82$ the mode with lower sign in Eq. (16) is unstable and purely growing, with maximum growth rate $(\mathrm{Im}\,\omega)^{max}/\omega_f = \sqrt{2/\sqrt{3} - 1} \approx 0.39$ occurring for $\nu_n^{max} = \sqrt{1/3} \approx 0.58$. Also, for

very intense beams with $\nu_n \to 0$, the normalized growth rate becomes $(\mathrm{Im}\,\omega)/\omega_f \simeq \bar{\nu}/\nu_0$. In Fig. 1(a), the normalized growth rate $(\mathrm{Im}\,\omega)/\omega_f$, plotted as a function of the normalized tune depression $\bar{\nu}/\nu_0$ [Eq. (16)], is compared with the numerical results described in Sections 3 and 4. Despite the approximations made in the present simplified model, the agreement is reasonably good.

3. Description of beam eigenmode and spectra (bEASt) code

As discussed in Section 1, it is important to extend theoretical studies of the kinetic stability properties of anisotropic beams to distribution functions other than the KV distribution. This is because the KV distribution has a highly unphysical (inverted) population in transverse phase-space variables, which provides the free energy to drive collective instabilities at sufficiently high beam intensity that are intrinsic to this inverted population [2–4]. This, of course, can mask the effects of anisotropy-driven instabilities.

For an arbitrary equilibrium distribution one cannot solve the stability problem analytically and must employ numerical techniques. To investigate the stability properties numerically, we make use of the linear eigenmode method, which searches for the roots of the matrix dispersion relation, as implemented in the bEASt code.

Next, we briefly outline the derivation of the matrix dispersion relation for the Harris-like instability [11,13] in intense particle beams for electrostatic perturbations about the thermal equilibrium distribution with temperature anisotropy ($T_{\perp b} > T_{\parallel b}$) described *in the beam frame* ($V_b = 0$ and $\gamma_b = 1$) by the self-consistent axisymmetric Vlasov equilibrium [15,17]

$$f_b^0(r,\mathbf{p}) = \frac{\widehat{n}_b}{(2\pi m_b)^{3/2} T_{\perp b} T_{\parallel b}^{1/2}} \times \exp\left(-\frac{H_\perp}{T_{\perp b}} - \frac{p_z^2}{2m_b T_{\parallel b}}\right). \tag{17}$$

Here, $H_\perp = p_\perp^2/2m_b + (1/2)m_b\omega_f^2(x^2+y^2) + e_b\phi^0(r)$ is the single-particle Hamiltonian for transverse particle motion, $p_\perp = (p_x^2 + p_y^2)^{1/2}$ is the transverse particle momentum, $r = (x^2+y^2)^{1/2}$ is the radial distance from the beam axis, and $\phi^0(r)$ is the equilibrium space-charge potential determined self-consistently from Poisson's equation,

$$\frac{1}{r}\frac{\partial}{\partial r} r \frac{\partial \phi^0}{\partial r} = -4\pi e_b n_b^0 \tag{18}$$

where $n_b^0(r) = \int \mathrm{d}^3 p f_b^0(r,\mathbf{p})$ is the equilibrium number density of beam particles. For simplicity, the analysis is carried out in the beam frame ($V_b = 0$ and $\gamma_b = 1$). Furthermore, setting $\phi^0(r=0) = 0$, the constant $\widehat{n}_b$ occurring in Eq. (17) can be identified with the on-axis density $n_b^0(r=0)$, and the constants $T_{\perp b}$ and $T_{\parallel b}$ can be identified with the transverse and longitudinal temperatures (energy units), respectively.

For present purposes, we consider small-amplitude electrostatic perturbations of the form

$$\delta\phi(\mathbf{x},t) = \widehat{\delta\phi}(r)\exp(\mathrm{i}m\theta + \mathrm{i}k_z z - \mathrm{i}\omega t) \tag{19}$$

where $\delta\phi(\mathbf{x},t)$ is the perturbed electrostatic potential, k_z is the axial wavenumber, m is the azimuthal mode number and ω is the complex oscillation frequency, with $\mathrm{Im}\,\omega > 0$ corresponding to instability (temporal growth). We also assume that the beam is located inside a perfectly conducting cylindrical pipe with radius r_w. The linearized Poisson equation can be expressed as

$$\frac{1}{r}\frac{\partial}{\partial r} r \frac{\partial}{\partial r}\widehat{\delta\phi}(r) - k_z^2\widehat{\delta\phi}(r) - \frac{m^2}{r^2}\widehat{\delta\phi}(r) = -4\pi e_b \int \mathrm{d}^3 p\, \widehat{\delta f_b}(r,\mathbf{p}) \tag{20}$$

with the boundary condition $\widehat{\delta\phi}(r=r_w) = 0$. Here $\widehat{\delta f_b}(r,\mathbf{p})$ is the Fourier amplitude of the perturbed distribution function $\delta f_b(r,z,\mathbf{p},t)$, i.e.,

$$\delta f_b(r,z,\mathbf{p},t) = \widehat{\delta f_b}(r,\mathbf{p})\exp(\mathrm{i}k_z z - \mathrm{i}\omega t). \tag{21}$$

The perturbed distribution function $\delta f_b(r,z,\mathbf{p},t)$ satisfies the linearized Vlasov equation [17].

$$\left\{\frac{\partial}{\partial t} + \mathbf{v}\cdot\frac{\partial}{\partial \mathbf{x}} - (e_b\nabla_\perp\phi^0 + m_b\omega_f^2\mathbf{x}_\perp)\cdot\frac{\partial}{\partial \mathbf{p}_\perp}\right\}\delta f_b = e_b\nabla\delta\phi\cdot\frac{\partial}{\partial \mathbf{p}} f_b^0. \tag{22}$$

In Eq. (20), we express the perturbation amplitude as $\widehat{\delta\phi}(r)=\sum_n \alpha_n\phi_n(r)$, where $\{\alpha_n\}$ are constants, and the complete set of vacuum eigenfunctions $\{\phi_n(r)\}$ is defined by $\phi_n(r)=A_nJ_m(\lambda_n r/r_w)$. Here, λ_n is the nth zero of $J_m(\lambda_n)=0$, and $A_n=\sqrt{2}/[r_wJ_{m+1}(\lambda_n)]$ is a normalization constant such that $\int_0^{r_w}\mathrm{d}r\,r\phi_n(r)\phi_{n'}(r)=\delta_{n,n'}$. We substitute $\widehat{\delta\phi}(r)=\sum_n\alpha_n\phi_n(r)$ into Poisson's equation (20) and operate with $\int_0^{r_w}\mathrm{d}r\,r\phi_{n'}(r)\cdots$. This gives the matrix dispersion equation [13]

$$\sum_n \alpha_n D_{n,n'}(\omega)=0 \tag{23}$$

where $D_{n,n'}(\omega)$ is defined by

$$D_{n,n'}(\omega)=\frac{J_{m+1}^2(\lambda_n)}{2}(\lambda_n^2+k_z^2r_w^2)\delta_{n,n'}+\chi_{n,n'}(\omega) \tag{24}$$

and the beam-induced susceptibility $\chi_{n,n'}(\omega)$ is defined by

$$\chi_{n,n'}(\omega)=-4\pi e_\mathrm{b}r_w^2\int_0^{r_w}\mathrm{d}r\,r\phi_{n'}(r)\int\mathrm{d}^3p\,\widehat{\delta f_\mathrm{b}^n}(r,\mathbf{p}). \tag{25}$$

Here, $\widehat{\delta f_\mathrm{b}^n}(r,\mathbf{p})$ is defined by Eqs. (21) and (22) with $\widehat{\delta\phi}\to\phi_n$.

Without presenting algebraic details, using the method of characteristics [11,13,17], the beam-induced susceptibility can be expressed as

$$\chi_{n,n'}(\omega)=\frac{r_w^2}{\lambda_\mathrm{d}^2}q_{n,n'}+\int_0^\infty\mathrm{d}s\exp\left(\mathrm{i}s\omega-\frac{s^2k_z^2T_\parallel}{2m_\mathrm{b}}\right)\times\left[\mathrm{i}\omega+\left(1-\frac{T_\parallel}{T_\perp}\right)\frac{sk_z^2T_\perp}{2m_\mathrm{b}}\right]Q_{n,n'}(s) \tag{26}$$

where

$$Q_{n,n'}(s)=\frac{1}{m_\mathrm{b}\lambda_\mathrm{d}^2}\sum_p\int\frac{\mathrm{d}P_\theta}{\omega_\mathrm{r}}\frac{\mathrm{d}H_\perp}{T_{\perp\mathrm{b}}}\exp\left[-\frac{H_\perp}{T_{\perp\mathrm{b}}}\right]\times(I_n^{p,m})^*I_{n'}^{p,m}\mathrm{e}^{-\mathrm{i}s(p\omega_\mathrm{r}+m\omega_\theta)}. \tag{27}$$

Here P_θ is the canonical angular momentum and $\lambda_\mathrm{d}^2=T_{\perp\mathrm{b}}/4\pi e_\mathrm{b}^2\widehat{n}_\mathrm{b}$ is the perpendicular Debye length-squared. In Eqs. (26) and (27), $q_{n,n'}$ and $I_n^{p,m}$ are defined by

$$q_{n,n'}=\int_0^1\mathrm{d}x\,xN(x)J_m(\lambda_nx)J_m(\lambda_{n'}x) \tag{28}$$

and

$$I_n^{p,m}(H_\perp,P_\theta)=\int_0^{T_\mathrm{r}}\frac{\mathrm{d}\tau}{T_\mathrm{r}}J_m\left[\frac{\lambda_nr(\tau)}{r_w}\right]\mathrm{e}^{-\mathrm{i}p\omega_\mathrm{r}\tau+\mathrm{i}m[\theta(\tau)-\omega_\theta\tau]}. \tag{29}$$

In the orbit integral in Eq. (29), $r(\tau)$ and $\theta(\tau)$ are the transverse orbits in the equilibrium field configuration such that $\theta(0)=0$ and $r(0)=r_{\min}(H_\perp,P_\theta)$ is the minimum radial excursion of the particle trajectory undergoing periodic motion with frequency $\omega_\mathrm{r}(H_\perp,P_\theta)=2\pi/T_\mathrm{r}$, and $\omega_\theta(H_\perp,P_\theta)=\theta(T_\mathrm{r})/T_\mathrm{r}$ is the average frequency of angular rotation. In Eq. (28), $(\,)^*$ denotes complex conjugate, and $N(x)=n_\mathrm{b}^0(xr_w)/\widehat{n}_\mathrm{b}$ is the normalized density profile, where $n_\mathrm{b}^0(r)=\int\mathrm{d}^3pf_\mathrm{b}^0(r,\mathbf{p})$. The condition for a nontrivial solution to Eq. (23) is

$$\det\{D_{n,n'}(\omega)\}=0 \tag{30}$$

which plays the role of a matrix dispersion relation that determines the complex oscillation frequency ω.

The dispersion relations (23) and (30) can be used to investigate detailed electrostatic stability properties for beams with temperature anisotropy ($T_{\perp\mathrm{b}}/T_{\perp\mathrm{b}}<1$) for a wide range of normalized axial wavenumbers (k_zr_b) and normalized tune depression $\bar{\nu}/\nu_0$. For sufficiently large values of k_zr_b, the large temperature anisotropy ($T_{\parallel\mathrm{b}}/T_{\perp\mathrm{b}}\ll1$) in Eqs. (23) and (30) provides the free energy to drive the classical Harris-type instability [1], generalized here to include finite transverse geometry and beam space-charge effects.

The bEASt code solves Eq. (23) in several steps. First, the particle orbits $r(\tau)$ and $\theta(\tau)$ in the equilibrium field configuration are calculated for one complete oscillation period T_r and the frequencies $\omega_\mathrm{r}(H_\perp,P_\theta)$ and $\omega_\theta(H_\perp,P_\theta)$ are obtained. Next, a fast Fourier transform (FFT) is used to calculate the orbit integrals in Eq. (29). In the next step, the matrices $Q_{n,n'}(s)$ [Eq. (27)] and $q_{n,n'}$ [Eq. (27)] are calculated, stored, and then used repeatedly to recalculate the beam-induced susceptibility [Eq. (26)] and dispersion matrix [Eq. (24)] during the search for the eigenvector of the dispersion matrix $D_{n,n'}(\omega)$ [Eq. (23)] with zero eigenvalue. Note that the matrices $Q_{n,n'}(s)$ and $q_{n,n'}$ are calculated only once, thanks to the separation

of the particle variables $(H_\perp, P_\theta, r, \theta)$ from the dispersion equation variables ω and k_z in Eq. (26). The typical number of particle trajectories used in the calculations is 300, with 16 time steps during one oscillation period T_r, which is significantly less than the number of particles and times steps used in PIC simulations [11–14]. The method described here works well for finding the unstable modes, or slightly damped modes. For highly damped modes, an accurate integration in Eq. (26) requires calculation of the matrix $Q_{n,n'}(s)$ for values of $s > |\mathrm{Im}\,\omega|/(k_z^2 T_\perp/m_b)$, which can be computationally extensive.

4. Numerical results

Typical numerical results obtained using the bEASt code are presented in Figs. 1–4 for the case where $r_w = 3r_b$. Fig. 1 shows the normalized growth rate $(\mathrm{Im}\,\omega)_{max}/\omega_f$ and real frequency $(\mathrm{Re}\,\omega)_{max}/\omega_f$ at maximum growth plotted versus the normalized tune depression $\bar{\nu}/\nu_0$ for $T_{\|b}/T_{\perp b} = 0$ and $m = 0, 1$. For $m = 0$, there are two distinct unstable modes. One is the fastest growing mode for $\bar{\nu}/\nu_0 > 0.55$, and the other is the fastest growing mode for $\bar{\nu}/\nu_0 < 0.55$. The approximate expression [Eq. (16)] for the normalized growth rate $(\mathrm{Im}\,\omega)_{max}/\omega_f$ is also plotted in Fig. 1a (thick solid curve) for comparison. The $m = 1$ dipole mode has the highest growth rate, $(\mathrm{Im}\,\omega)/\omega_f \simeq 0.34$, for $\bar{\nu}/\nu_0 \simeq 0.62$. The instability is absent for $\bar{\nu}/\nu_0 > 0.82$ for the choice of parameters in Fig. 1. The real frequency $(\mathrm{Re}\,\omega)/\omega_f$ of the unstable mode with azimuthal number $m = 1$ is zero, and is not plotted in Fig. 1. Moreover, the real frequency is plotted only for the most unstable modes.

Fig. 2 shows the normalized growth rate $(\mathrm{Im}\,\omega)/\omega_f$ plotted versus the normalized wavenumber $k_z r_b$ for the normalized tune depression $\bar{\nu}/\nu_0 = 0.3$ and several values of the temperature ratio $T_{\|b}/T_{\perp b} = 0.0, 0.01, 0.05$. Figs. 2(a) and (b) correspond to azimuthal mode numbers $m = 0$ and $m = 1$, respectively. As expected, the instability is present only for short-wavelength perturbations with $k_z^2 r_b^2 > 1$, and finite $T_{\|b}$ effects introduce a finite bandwidth in $k_z r_b$ for instability, since the modes with large values of $k_z r_b$ are stabilized by longitudinal Landau damping. Also, the unstable dipole mode with $m = 1$ is purely growing.

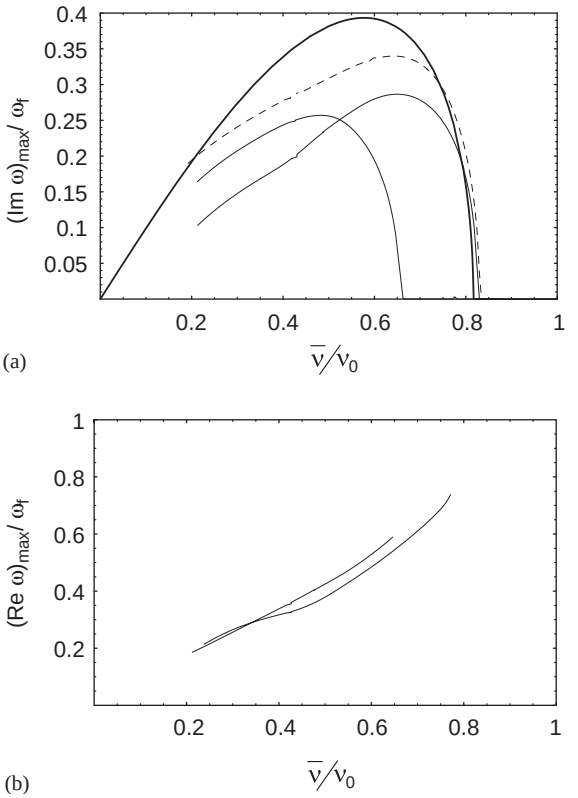

Fig. 1. Plots of the normalized growth rate $(\mathrm{Im}\,\omega)_{max}/\omega_f$ and real frequency $(\mathrm{Re}\,\omega)_{max}/\omega_f$ at maximum growth versus normalized tune depression $\bar{\nu}/\nu_0$ for $T_{\|b}/T_{\perp b} = 0$ and $m = 0$ (solid curve) and $m = 1$ (dotted curve). Thick solid curve corresponds to Eq. (16).

The normalized eigenfunctions $\mathrm{Re}\,\delta\widehat{\phi}(r)$ and $\mathrm{Im}\,\delta\widehat{\phi}(r)$ corresponding to two values of normalized depressed tune $\bar{\nu}/\nu_0 = 0.3, 0.6$ and two values of azimuthal mode number $m = 0, 1$ for $k_z r_b = 20$ and infinite anisotropy $T_{\|b}/T_{\perp b} = 0$ are plotted versus r/r_w in Fig. 3. Note, that for smaller normalized depressed tune, the eigenfunctions become localized near the beam edge. An important characteristic of the instability is the longitudinal threshold temperature $T_{\|b}^{th}$ for the onset of instability normalized to the transverse temperature $T_{\perp b}$. Due to accuracy limitations in the bEASt code, we define the threshold as the value of $T_{\|b}/T_{\perp b}$ at which the maximum

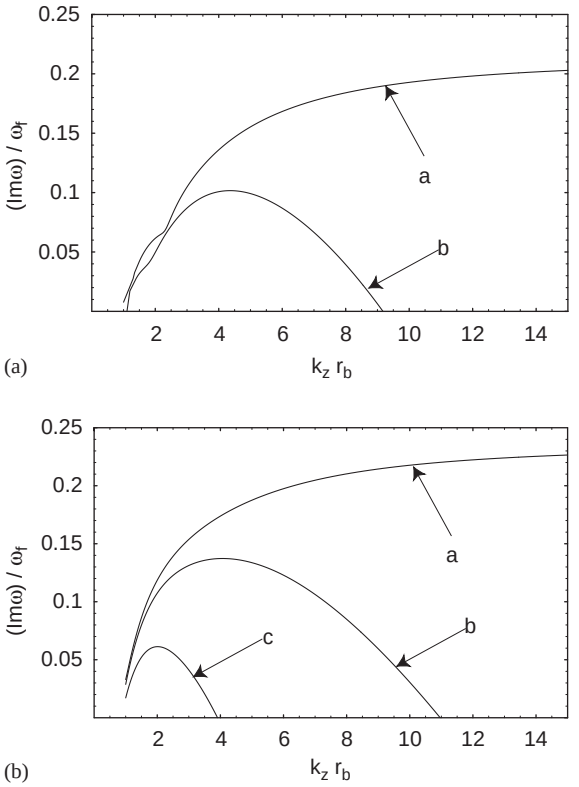

Fig. 2. Plots of the normalized growth rate $(\mathrm{Im}\,\omega)/\omega_f$ versus $k_z r_b$ for $\bar{v}/v_0 = 0.3$ and several values of the temperature ratio $T_{\|b}/T_{\perp b} = 0, 0.01, 0.05$ (curves a,b and c). Here, figures (a) and (b) are for azimuthal mode number $m = 0$ and $m = 1$, respectively.

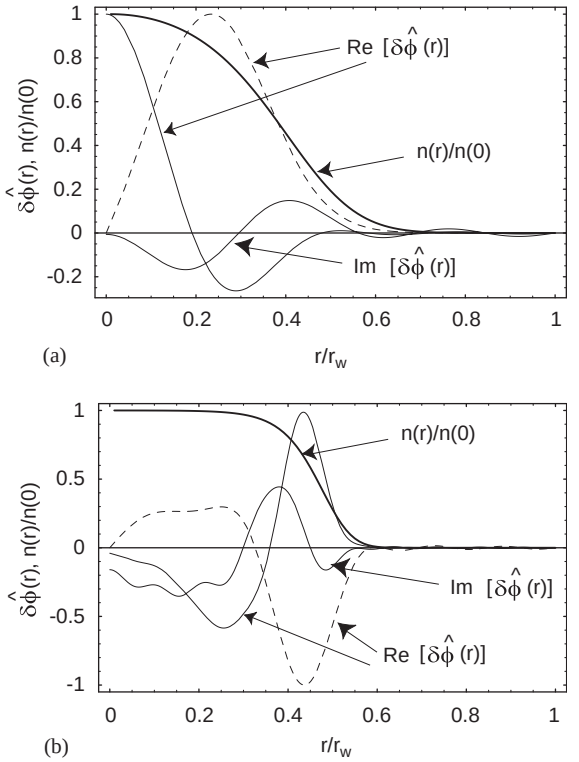

Fig. 3. Plots of the normalized eigenfunctions $\mathrm{Re}[\delta\widehat{\phi}(r)]$ and $\mathrm{Im}[\delta\widehat{\phi}(r)]$ for the most unstable modes versus r/r_w corresponding to $m = 0$ (solid curves) and $m = 1$ (dotted curve) and two values of normalized depressed tune, $\bar{v}/v_0 = 0.6$ (a) and $\bar{v}/v_0 = 0.3$ (b). Here, $T_{\|b}/T_{\perp b} = 0$ and $k_z r_b = 20$. Thick solid curve corresponds to normalized density profile $n(r)/n(0)$.

normalized growth rate becomes less than $(\mathrm{Im}\,\omega)_{\max}/\omega_f < 0.01$. This quantity is plotted in Fig. 4 versus the normalized tune depression $\bar{v}/v_0$ for two values of azimuthal number corresponding to $m = 0, 1$. Note from Fig. 4 that the maximum threshold value, $T_{\|b}/T_{\perp b} = 0.11$, is achieved for moderately intense beams with $\bar{v}/v_0 = 0.4$.

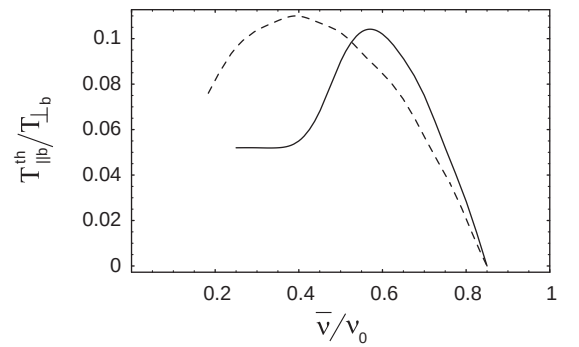

Fig. 4. Longitudinal threshold temperature $T_{\|b}^{th}$ for the onset of instability normalized to the transverse temperature $T_{\perp b}$ is plotted versus normalized tune depression $\bar{v}/v_0$ for two values of the azimuthal mode number, $m = 0$ (solid line) and $m = 1$ (dotted line).

5. Conclusions

The bEASt code, which solves the matrix dispersion relation Eq. (23) for electrostatic perturbations in intense particle beams, has been used to investigate the stability properties of intense charged particle beams with large temperature anisotropy ($T_{\|b}/T_{\perp b} \ll 1$) over a wide

range of normalized tune depression, $0.2 < \bar{\nu}/\nu_0 < 1$. The numerical results clearly show that intense beams with $\bar{\nu}/\nu_0 < 0.82$ are linearly unstable to short-wavelength perturbations with $k_z^2 r_b^2 \geqslant 1$. The instability is kinetic and is due to the coupling of the particles transverse betatron motion with the longitudinal plasma oscillations excited by the perturbation. The normalized instability growth rate is a maximum for moderately intense beams with $\bar{\nu}/\nu_0 \sim 0.62$ and is proportional to the normalized tune, i.e., $\mathrm{Im}\,\omega/\omega_f \approx \bar{\nu}/\nu_0$ for $\bar{\nu}/\nu_0 \ll 1$. The most unstable mode is found to be a purely growing dipole mode with normalized growth rate $\mathrm{Im}\,\omega/\omega_f \simeq 0.34$ for $\bar{\nu}/\nu_0 \simeq 0.62$ and $T_{\parallel b}/T_{\perp b} = 0$. The instability is stabilized by longitudinal Landau damping whenever the ratio of the longitudinal and transverse temperatures satisfies $T_{\parallel b}/T_{\perp b} > 0.11$.

Acknowledgement

This research was supported by the U.S. Department of Energy.

References

[1] E.G. Harris, Phys. Rev. Lett. 2 (1959) 34.
[2] T.-S. Wang, L. Smith, Part. Accel. 12 (1982) 247.
[3] R.L. Gluckstern, in: M.R. Tracy (Ed.), Proceedings of the 1970 Proton, Linear Accelerator Conference, Batavia, IL, National Accelerator Laboratory, Batavia, IL, 1971, p. 811.
[4] T.-S. Wang, Phys. Rev. ST Accel. Beams 7 (2004) 024201.
[5] A. Friedman, D.A. Callahan, D.P. Grote, A.B. Langdon, I. Haber, Bull. Am. Phys. Soc. 35 (1990) 2121.
[6] A. Friedman, R.O. Bangerter, D.A. Callahan, D.P. Grote, A.B. Langdon, I. Haber, in: P.A. Martin (Ed.), Proceedings of the Second European Particle Accelerator Conference, vol. 2, 1990, p. 1699.
[7] A. Friedman, D.P. Grote, I. Haber, Phys. Fluids B 4 (1992) 2203.
[8] S.M. Lund, D.A. Callahan, A. Friedman, D.P. Grote, I. Haber, T.F. Wang, in: C.E. Eyberger, R.C. Pardo, M.M. White (Eds.), Proceedings of XIX International Linear Accelerator Conference, Chicago, Argone National Laboratory, Argone, Illinois, 1998, p. 372.
[9] S.M. Lund, J.J. Barnard, G.D. Craig, A. Friedman, D.P. Grote, T.S. Sangster, W.M. Sharp, S. Eylon, T.T. Fessenden, E. Henestroza, S. Yu, I. Haber, Nucl. Instr. and Meth. A 415 (1998) 345.
[10] I. Haber, A. Friedman, D.P. Grote, S.M. Lund, R.A. Kishek, Phys. Plasmas 6 (1999) 2254.
[11] E.A. Startsev, R.C. Davidson, H. Qin, Phys. Plasmas 9 (2002) 3138.
[12] E.A. Startsev, R.C. Davidson, H. Qin, Laser Part. Beams 20 (2002) 585.
[13] E.A. Startsev, R.C. Davidson, H. Qin, Phys. Rev. ST Accel. Beams 6 (2003) 084401.
[14] H. Qin, R.C. Davidson, W.W. Lee, Phys. Rev. ST Accel. Beams 3 (2000) 084401; H. Qin, R.C. Davidson, W.W. Lee, Phys. Rev. ST Accel. Beams 3 (2000) 109901.
[15] R.C. Davidson, Phys. Rev. Lett. 81 (1998) 991.
[16] S.E. Parker, W.W. Lee, Phys. Fluids B 5 (1993) 77.
[17] R.C. Davidson, H. Qin, Physics of Intense Charged Particle Beams in High Energy Accelerators, World Scientific, Singapore, 2001, and references therein.